A mesoscale interface approach to modelling fractures in concrete for material investigation

Citation for published version:
Zhou, R & Lu, Y 2018, 'A mesoscale interface approach to modelling fractures in concrete for material investigation', *Construction and Building Materials*, vol. 165, pp. 608-620.
https://doi.org/10.1016/j.conbuildmat.2018.01.040

Digital Object Identifier (DOI):
10.1016/j.conbuildmat.2018.01.040

Published In:
Construction and Building Materials

A mesoscale interface approach to modelling fractures in concrete for material investigation

Rongxin Zhou and Yong Lu*

Institute for Infrastructure and Environment, School of Engineering, the University of Edinburgh, Edinburgh EH9 3JL, UK

* Corresponding author. Email: yong.lu@ed.ac.uk

Abstract

Advanced computational modelling can provide a powerful tool for material investigation and characterisation. For concrete materials, appropriate description of the heterogeneity and realisation of complex fractures are two challenging aspects in high fidelity numerical simulations. This paper presents a new mesoscale model for concrete with the ability of simulating natural evolution of fracture at the interface between the aggregates and mortar matrix and without restriction to the loading conditions. To this end, a combined cohesive and contact interface approach is employed. The contact-friction process at a fractured interface is treated as an independent process that complements the general cohesive law, thus allowing the closure of cracked surfaces and the development of residual shear resistance in a realistic manner. Parametrisation is conducted to examine the effects of pertinent interface parameters on the macroscopic behaviour of concrete. The modelling approach is demonstrated to be capable of simulating the behaviour of concrete under a variety of loading conditions, including confined and dynamic compression. The new mesoscale model provides a comprehensive numerical means for investigating into the micro-mesoscale mechanisms underlying the macroscopic behaviour of concrete.

Keywords: concrete material; heterogeneity; fracture; mesoscale model; cohesive zone; contact model.

1. Introduction

Concrete is a non-homogeneous composite with large heterogeneities. The behaviour of concrete is fundamentally affected by the fracture mechanisms, particularly at interfaces between aggregates and the mortar matrix, i.e. the interfacial transition zone or ITZ. Modelling of concrete is complicated because of the development of fractures, in that at the initial stage concrete behaves primarily like a heterogeneous continuum solid, but when fractures grow it gradually becomes discontinuous.

Modelling of concrete at the mesoscale makes it possible to describe the composition of the material, and it has been a subject of continuous interest in the research community concerning brittle and quasi-brittle solids (e.g. [1-3]). As summarised in [4], three distinctive approaches have been employed in mesoscale modelling of concrete, namely lattice model, discrete element model (DEM), and continuum finite element (FE)-based model.

A key factor that determines the extent to which a mesoscale model may be capable of realistically representing the intrinsic failure mechanisms is the modelling of fractures. In lattice models [5-6], fracture is generally represented by continuingly breaking the lattice members, which may be beam or truss elements, when a failure criterion is met. This approach is suitable for crack opening; but it cannot accommodate possible crack closure. The discrete element or particle models possess inherent advantages in accommodating crack-induced discontinuity; however its ability in modelling the continuum and partially damaged states of concrete is subject to the equivalent description of the continuum properties, and such equivalent description is difficult to generalize for different stress conditions [4].

Finite element-based mesoscale model is well suited for representing the intact concrete as it is essentially a non-homogenous continuum. As in the general FE model of concrete, cracks may be described using either a smeared or a discrete approach. However, previous research has shown some well-known issues with the standard continuum elements, such as the mesh size dependency and the limited deformation modes in the smeared crack approach when the softening behaviour is involved [7].

The incorporation of cohesive interface elements within a finite element framework makes it possible to follow the initiation and propagation of multiple cracks. These interface lines can branch, coalesce, and eventually form new free surfaces. The mechanical properties of the interface can generally be described using a cohesive law, which represents a gradual loss of the strength with increasing separation and can also be related to the work of separation, or fracture energy that is required for the complete formation of a free surface [8]. Figure 1 depicts the formation of a separation (crack) over an interface with cohesive zone elements.

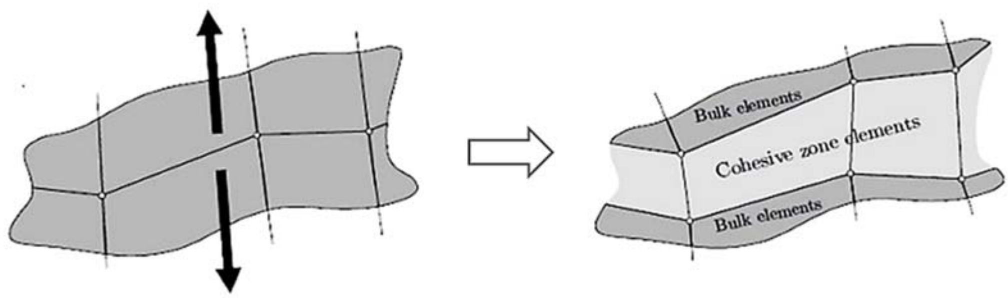

Fig. 1. Cohesive elements along mesh lines (after [8])

As the macroscopic failure in concrete is much dependent on the interface between aggregate and mortar, a sound representation of the mechanical properties and the fracture at the ITZ is crucial for a realistic modelling of the mesoscopic damage mechanisms for concrete-like materials. Therefore in the present study the focus has been placed to develop a holistic interface approach to capture the complex damage process at the ITZ for any stress conditions.

It is generally understood that the real ITZ has a very thin thickness of 20-50 μm [9-10], and it has a different mechanical property from the cement paste. Because of its thin thickness, it may be reasonably represented by zero-thickness cohesive elements.

The adequacy of using cohesive elements for modelling the ITZ in a general mesoscale model depends upon the capacity of the cohesive elements in catering to complex stress conditions. A classical cohesive model is suited for modelling the interface failure involving model I and mode II fractures. Applying this cohesive element model proves to work well under tension-dominated loading, but it performs poorly in other loading conditions including axial compression [2]. The reason is deemed to relate to the inability of the cohesive element in representing the shear failure of the ITZ under a complex stress condition.

Some other techniques have also been developed in attempt to address the coupled effect of normal and shear stresses at a cohesive interface. An interface element which incorporates the interaction of cohesion, tensile strength and the friction angle in a constitutive model has been proposed [7] to investigate the concrete fracture mechanism under complex loading conditions. The main feature of this interface element is that it introduces a friction dissipative mechanism between two potential crack surfaces into the cohesive law intrinsically. By defining several loading fracture surfaces at different loading stages with shape parameters, such a model can generally simulate the whole process from fracture to pure friction. However some of the parameters used in the model cannot be obtained easily and some are also case-dependent. Moreover, as Ruiz et al. [11] suggested, the contact and friction process should be regarded as independent phenomena outside cohesive law. This is because physically fracture and friction are two independent processes, and in particular the presence of friction may result in a steady frictional resistance while the normal cohesive strength simultaneously weakens. Thus a contact-friction algorithm is deemed to be more appropriate to represent the interaction resistance at cracked surfaces.

In this paper, a holistic interface approach combining the cohesive mechanism with the contact-friction mechanism is developed to explicitly represent the behaviour of ITZ in a mesoscale concrete model. Relatively simple and explicit physical laws are employed for individual mechanisms. In conjunction with the mesoscale description of the complex geometric interface between the mortar and random aggregates, which allows for the fracture path to develop in a more realistic manner, the combined framework provides a comprehensive method to capture the detailed damage processes in concrete under all general loading conditions. The application of the model for material investigations is demonstrated by numerical simulation of concrete under different loading conditions in comparison with experimental observations.

2. Modelling approach for ITZ in a mesoscale framework

2.1 Overview of the mesoscale model and meso-structure generation

The present study is focused on fracture modelling of concrete in a two-dimensional (2D) mesoscale model framework, with a holistic interface description for the ITZ. The mesoscale structure of concrete is represented by a stochastic distribution of coarse aggregates embedded in the mortar matrix. The aggregates are modelled by random polygon particles, and the nominal size of the individual aggregates obeys a given grading curve. The generation of the mesoscale geometry follows a commonly adopted take-and-place procedure [12], satisfying non-overlapping and minimum gap requirements. The density of the aggregates can be controlled by specifying a volume ratio, e.g. 45% in this paper. For normal concrete, the coarse aggregates are defined as those with a minimum nominal size of 4.75 mm [1]. Herein the procedure is programmed using MATLAB.

After the generation of the mesoscale structure, the geometrical data can be brought into a finite element meshing processor. In the present study, ANSYS pre-processor is used to perform the FE-meshing. Figure 2 illustrates a typical mesoscale model geometry. In this figure, only two material components, namely aggregates and the mortar matrix, are shown. The third component, i.e. the interface transition zone (ITZ) between aggregates and mortar matrix can be created subsequently. To overcome the issues with modelling the ITZ with an equivalent thin layer of solid elements as mentioned earlier, herein the ITZ is explicitly modelled with a combined classic zero-thickness cohesive interface element and a contact algorithm. The creation of such a combined interface element will be discussed in the next section.

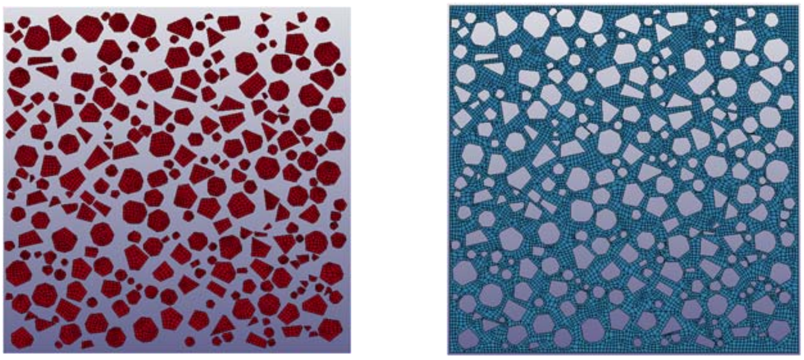

(a) Aggregates (b) Mortar matrix

Fig. 2. Mesoscale model of concrete and FE mesh

2.2 Modelling of ITZ with a cohesive zone model

The main advantage of using a cohesive zone model for fracture is that it can simulate the gradual process of the cracking surface separation with a cohesive law. A typical cohesive law relates the relative displacement of two associated points of the interface (δ) to the traction force per unit area (T) that is needed for separation. Different cohesive laws may be defined for the normal and tangential directions, respectively, but in most models the cohesive laws for the two directions are coupled, meaning that both the normal and tangential tractions (T_n, T_t) depend on both the normal and tangential opening displacements (δ_n, δ_t).

2.2.1 Cohesive elements insertion

In the present mesoscale model the boundaries between aggregates and mortar matrix are all treated as the potential crack surfaces, and the zero-thickness elements are inserted. To achieve this, a duplicate set of the nodes are required at all the interface locations. The original nodes and the duplicated nodes form the two potential cracking surfaces of cohesive elements, and they can separate during crack propagation. Each pair of two nodes at the same location (see Figure 3) will be constrained by a separation-traction law.

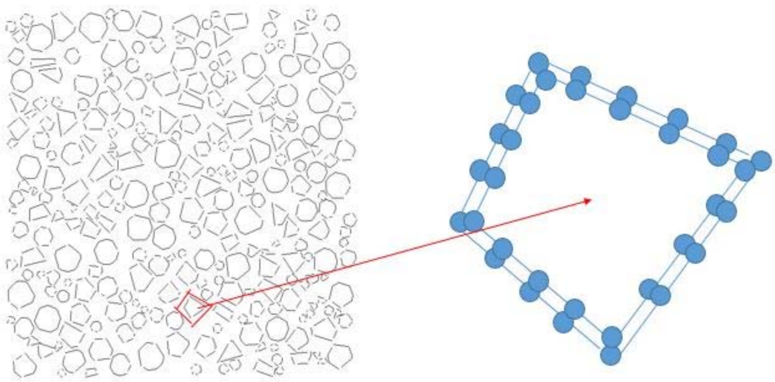

Fig. 3. Illustration of zero-thickness interface elements insertion

Depending on the response of the cohesive surface prior to the development into the softening stage, two types of cohesive zone approaches may be considered when the cohesive elements are inserted, namely intrinsic and extrinsic cohesive zone models [13]. Intrinsic cohesive elements are embedded in the discretized structure at the beginning of the simulation, and during the whole simulation process the mesh connectivity remains unchanged. Extrinsic cohesive models, on the other hand, insert the cohesive elements adaptively into the mesh, which means the cohesive elements are inserted only when the boundary stresses reach the critical material strength. At this juncture, it is worth noting that in the mesoscale model the crack paths will be subject to natural regularisation due to the presence of the aggregates, and hence can be highly irregular. Therefore in the present study we adopt the intrinsic cohesive model approach for the ITZ.

2.2.2 Cohesive constitutive model

The cohesive constitutive model used in the present study is a typical simple bilinear cohesive model for modelling the interface failure involving interaction between model I and model II fractures [14]. It considers the irreversible damage and allows for independent definitions of the constitutive relations for different fracture modes of tension and shear. The constitutive laws used for modelling mode I and mode II fracture are depicted by the curves in the 'traction-δ_I' and 'traction-δ_{II}' planes respectively, as it is shown schematically in Figure 4. Only some key parameters such as the stiffness, K_N and K_S, the peak tractions σ_I^P,σ_{II}^P and the fracture energies G_{IC}, G_{IIC} in the normal and shear directions respectively, need to be specified. Generally the interface layers in a mesoscale concrete model will not be subjected to just pure Mode I or Pure Mode II loading. Therefore, a mixed-mode needs to be specified to couple the two independent models. In the present study, the representative power law [14], in which a mixed-mode initiation displacement and the ultimate mixed-mode displacement (total failure) can be correspondingly calculated, is employed.

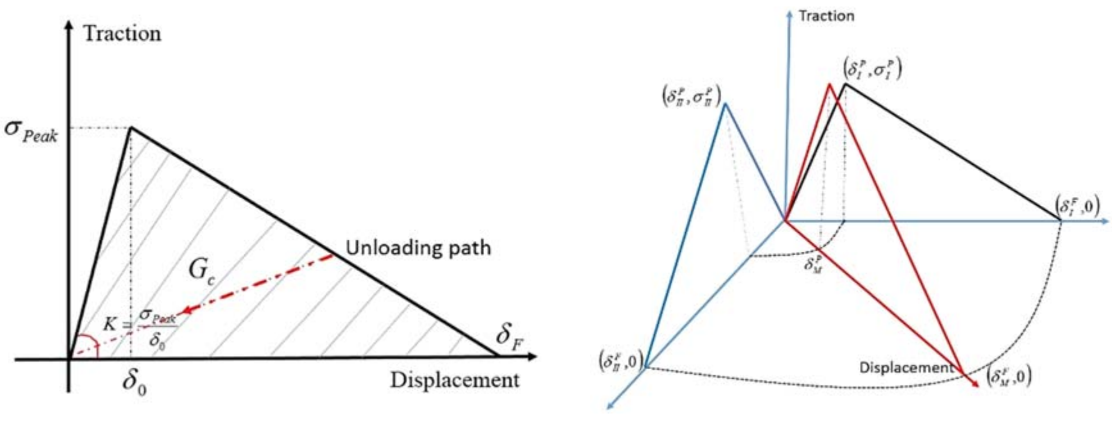

(a) Pure mode (b) Mixed mode

Fig. 4. Illustration of mixed-mode constitutive law for cohesive elements (after [14])

2.3 Incorporation of contact-friction mechanism

As mentioned earlier the performance of the traditional cohesive model becomes poor if the interface is subject to a compressive or shear loading while a crack is developing. This is deemed to be due to a lack of representation of the contact and friction mechanism. To revolve this problem, in the present model a penalty-based algorithm is adopted to handle the contact between two cracked surfaces of an interface element. The penalty-based algorithm proves to be stable and it is also easy to implement in FEM [15].

A sketch of the penalty-based contact algorithm is shown in Figure 5. An equivalent elastic, compression-only spring is placed in the normal direction to resist penetration. Each slave node is checked for penetration through the master surface. If there is no penetration nothing is done but when it does penetrate, an interface force is applied between the slave node and its contact point. The magnitude of this force depends on the amount of penetration with a linear relationship.

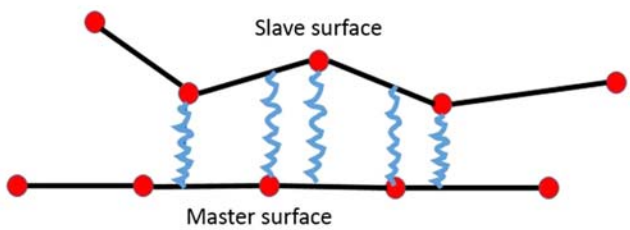

Fig. 5. Sketch of the penalty-based contact method

In the tangential direction, a friction stress is introduced according to the Coulomb Friction law. Two types of friction stress limit, namely the maximum static friction and the kinetic friction are both considered in present study. While the friction stress developed in the kinetic stage can be easily defined by a linear relationship to the normal stress, the determination of the limit static friction stress, which develops before a complete de-cohesion (loss of cohesion), is not straightforward and warrants a special consideration. This will be discussed in association with the combined model in what follows.

2.4 Cohesive-plus-contact model

As stated earlier, we simulate cohesive fracture and the contact-friction as two independent mechanisms. Depending on the stress condition, an interface element may develop into a full crack state without activating any contact frictional effect, or it may involve degradation of cohesion and friction sliding at the same time. To enable both mechanisms to work, it is important to define how friction should develop while the cohesion degrades, which indicates crack opening at the same interface.

In the literature the treatment of the transition stage from cohesion to pure friction at an interface varies, from the very beginning to a complete de-bonding of the cohesive zone. Tvergaad [16] introduced the friction mechanism to a cohesive law such that the friction takes effect only when de-cohesion is fully attained. This approach can successfully predict the residual stress after de-bonding but cannot model the additional load-carrying capacity due to the fracture roughness. Chaboche et al. [17] modified the interface law by introducing a friction term from the very beginning. This model effectively treated the friction mechanism as a kinematic hardening effect with a decreasing hardening modulus as the damage progresses, thus it is capable of predicting the additional load capacity due to friction. More recent works on this topic have focused on coupling the initiation of friction with the onset of fracture, for instance [18-20].

A general feature among the above mentioned studies is that the friction effect between two potential crack surfaces is incorporated into the cohesive law internally. This would result in a more complex cohesive constitutive law and the equivalent parameters can be sensitive to specific loading conditions.

In the present paper, the physical process of contact and friction at a fractured interface is modelled independently and it complements the general cohesive law, thus providing a framework that allows the distinctive mechanisms of cohesion, contact (closure of cracked surfaces) and friction to develop directly. Each mechanism has a clear physical meaning and this paves the way for the determination of the relevant parameters for each mechanism in a more straightforward manner. Together with a more realistic description of the topology of the fracture path in the mesoscale model, this enables a realistic simulation of the complex fracture and degradation process in concrete suitable for the material investigations.

Preliminary explorations in the present study revealed that simply adding the cohesive and contact-friction components together cannot yield satisfactory results; the model could easily become unstable and produce erroneous results. This is most probably because traditional contacts can only introduce the frictional resistance after the complete failure of cohesion, causing the stability issue and an inability to predict the additional force-transfer capacity due to friction during the transition stage.

To overcome this problem, we propose to introduce a continuous friction mechanism which starts from the beginning of loading. To reflect different degree of the friction engagement at different states of the interface, the whole process is subdivided into three stages. Stage 1 corresponds to the undamaged state of the cohesive element. During this stage, the cohesion dominates and the friction term is negligible. Stage 2 is the process from the onset of fracture until full de-cohesion. In this stage, the friction and the remaining cohesion act on the same interface simultaneously. The friction term acting at this stage may be viewed as a hardening effect leading to increased resistance capacity of the bulk material. It should be noted that the frictional movement during this stage is not an explicit interface slide but is constrained by the constitutive cohesion law that relates the friction force to the shear deformation, and therefore is effectively a static friction. The pure "sliding" friction stage is defined as stage 3. In this stage, the interface is fully separated thus the two contacting surfaces slide against each other with a frictional law. The friction at this stage is of kinetic character.

Figure 6 illustrates the behaviour of the combined cohesion and friction model with three distinctive stages of the response, as obtained from a representative numerical result. The determination of the pertinent parameters is discussed in the next section.

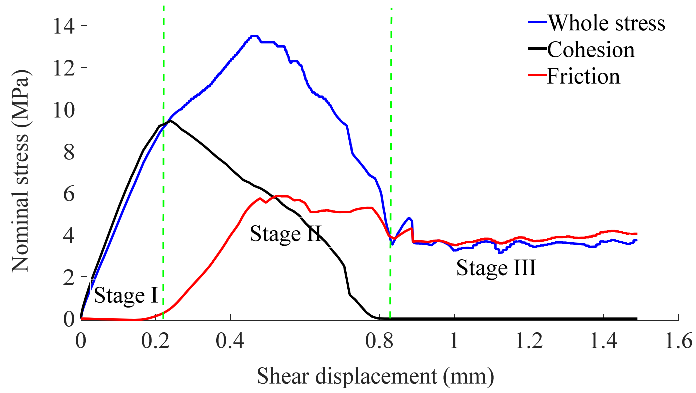

Fig. 6. Evolution of the combining mechanism during different stages

2.5 Parameter settings in the combined interface model

In addition to parameters which may be related to the basic material properties, such as the cohesive strengths and kinetic friction coefficient, appropriate initial stiffness and the static friction stress limit (*SFSL*) need be specified for the cohesive zone model. In addition, a suitable mesh size should also be chosen. This section examines the sensitivity of combined cohesive model to these parameters and discusses suitable values that may be adopted for the cohesive-plus-contact model.

A classical triplet shear experiment with lateral confining pressure is modelled for this investigation. The triplet experiment is commonly used in the testing of masonry materials to determine the ultimate shear strength of the mortar joints. Figure 7 shows a schematic of a finite element model simulating the experimental setup. The two side blocks (bricks) are supported rigidly at the lower edge, whereas the shear load is applied on the upper edge of the middle brick, which is simulated with a velocity boundary condition in the FE model. A constant normal pressure can be introduced by applying horizontal compression force on the side surfaces of the outer bricks. Considering symmetry, only half of the specimen is modelled.

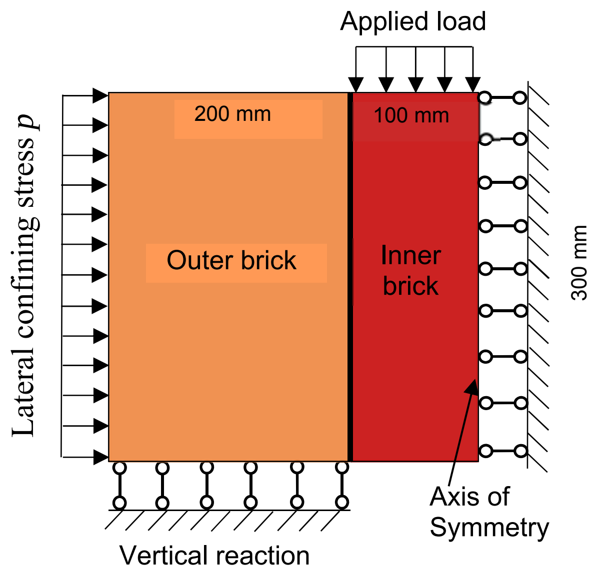

Fig. 7. Numerical model of shear test

For the sake of simplicity, the blocks are modelled as elastic with the following properties: Elastic modulus $E = 37$ GPa, Poisson's ratio $v = 0.2$ and mass density $\rho = 2.3 \times 10^{-3}\ \mathrm{g/mm^3}$. The interface layer is nonlinear and is modelled by the combined cohesive-plus-contact model. The parameters used in defining the interface model are as follows: peak traction in tension $\sigma_I^P = 2.7$ MPa, peak traction in shear $\sigma_{II}^P = 10.8$ MPa, fracture energy in mode-I $G_{IC} = 0.03$ N/mm, fracture energy in Mode-II $G_{IC} = 0.3$ N/mm and the kinetic friction coefficient $\mu = 0.7$. The mass density of the interface element is assumed as the same as that for the brick elements. It should be noted that these parameter values are in line with masonry but the simulation itself is generic for quasi-brittle solids and is not intended to tie with any physic experiment at this stage.

2.5.1 Mesh size

Simulations with five different mesh sizes, namely h = 50, 25, 10, 5, 2 mm have been conducted for the current specimen of 300mm in length. To maintain consistency across all models with different mesh sizes concerning the initial stiffness of the cohesive element, a sufficiently large stiffness $K_N = K_S = 10^6$ MPa / mm is used for all the cases. The overall results in terms of the nominal shear stress vs. shear displacement tend to converge with a mesh size no larger than 5 mm. A further examination of the effects of the mesh size on the two independent mechanisms (cohesion and friction) indicate that the cohesion tends to attain a generally convergent result when the mesh size is smaller than 25 mm, whereas the friction needs much finer mesh to approach the convergence. Generally a convergent result can be obtained for both cohesion and friction when the mesh size is no larger than 5 mm. Hence the mesh size 5 mm at the interface layer has been chosen for the simple shear test on the cohesive plus contact model hereinafter. .

2.5.2 Initial stiffness of cohesive element

The initial stiffness of the cohesive elements K is crucial for an adequate behaviour of the cohesive zone model. A general guideline in setting a suitable initial stiffness was proposed in Turon et al. [21] as:

$$K = \frac{\alpha E}{h_{mesh}} \tag{1}$$

where E is the Young's modulus for bulk element, h_{mesh} the mesh size of the bulk element and α the coefficient. Ideally, α should be set infinitively large to eliminate the artificial compliance due to the introduction of intrinsic cohesive element. However, an excessively large stiffness for the interface element may cause other numerical problems such as spurious oscillations of the traction [22]. Furthermore, large stiffness may also reduce the critical time step when an explicit dynamic algorithm is used, such as with LS-DYNA as used in the present study, which would increase the computing cost.

Five different interface stiffness parameters are examined here, namely, α = 0.05, 1, 10, 50 and 100. From the simulated nominal shear stress vs. shear displacement results, it can be observed that the stiffness generally has little influence on the global stress-displacement curves. Further examinations into the effect on the cohesion and friction shows that the effect of the stiffness on the cohesion response is also very limited. In contrast, the friction response is significantly influenced by the cohesive stiffness. As can be expected, when the cohesive stiffness is set relatively small (α = 0.05 or 1), the frictional mechanism is involved from the very beginning of the shear process. On the other hand, if the cohesive stiffness is set relatively large ($\alpha \geq 10$), the frictional mechanism comes into action only after a certain degree of 'separation'. It is interesting to find that when the stiffness parameter is larger than 10 the friction mechanism is not engaged until the shear displacement reaches about 0.2 mm, which is actually a typical threshold of fracture [23-24].

From the above results, it may be concluded that a relatively large value with $\alpha \geq 10$ needs to be employed for the cohesive stiffness in order to ensure that the friction starts from the onset of fracture. Considering the computational cost, which tends to increase with the increase of the cohesive stiffness as mentioned earlier 2, a value of $\alpha = 50$ is deemed to be appropriate and this value is used hereafter in the present study. It is worth mentioning that such a setting is consistent with the suggestions for cohesive zone models in some previous studies [21].

2.5.3 Friction stress limit

The contact friction algorithm is introduced to the whole fracture process from the very beginning. However before the complete loss of cohesion, the process is a combined de-cohesion and contact, in which the nodes that are initially at the same locations are still constrained by the cohesive constitutive law but they permit tangential motion with frictional sliding. At this stage, the model has no response to the Coulomb's kinetic friction law because there is essentially no 'free' relative slip between each pair of nodes. The friction stress that develops at this stage can be very large. It is reasonable and necessary to impose a static friction stress limit parameter (*SFSL*) in the contact-friction algorithm to set a limit value for the maximum static frictional stress. This can be implemented by integrating a tiebreak contact model with a traditional contact algorithm in the finite element framework.

The static friction limit value must ensure a realistic static friction and at the same time guarantee a smooth transition from the de-cohesion process to the pure friction stage. In this respect this parameter should on the one hand directly relate to the shear strength of the bulk material and on the other relate to the kinetic frictional coefficient of the contacting surface. However, the bulk materials on the two sides of a cohesive element are generally treated as simple linear-elastic material as in the present study. Based on preliminary analyses, it is suggested that the static friction limit could be set as two times of the cohesion strength (in the shear direction) for concrete-like materials, while a general kinetic frictional coefficient of around 0.7 is adopted.

3. Model performance and experimental verifications

3.1 Shear under different lateral pressures

When the combined cohesive and contact model is subjected to a mixed loading condition of shear with a certain level of normal pressure, the contact-friction effects will be involved and this is expected to increase the overall shear strength. The simulated shear stress vs. shear displacement curves for various levels of the normal compression pressure are shown in Figure

8(a). As expected, the current model successfully predicts a persistent increase in the shear strength as the normal compression increases. The residual shear strength which should be attributed to the basic friction stress effect (i.e. normal stress times the frictional coefficient) is also correctly obtained.

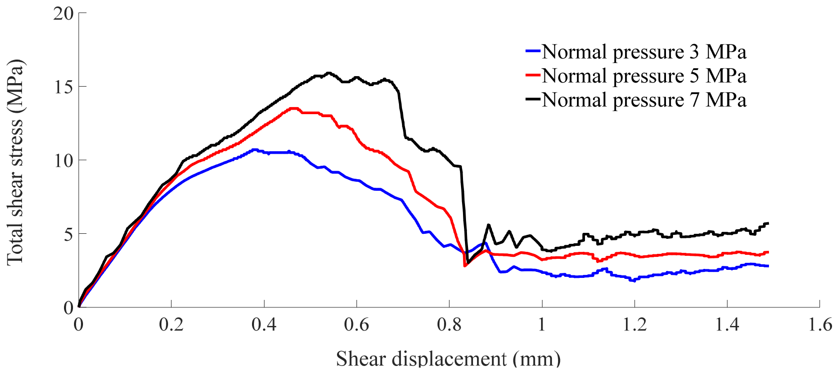

(a) Total shear under three different lateral pressure

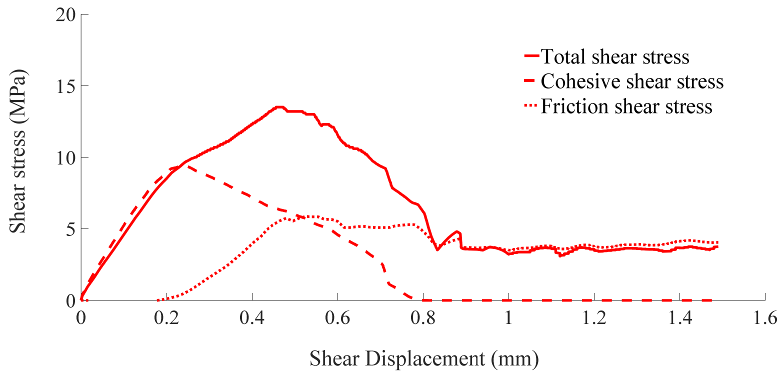

(b) Contributions to total shear under a lateral pressure of 5 MPa

Fig. 8. Simulated shear stress vs. shear displacement relationships

A further check on the evolution of cohesion and friction under a normal pressure of 5 MPa is presented in Figure 8(b). The other two cases follow the same trend. As it is shown, the principle of the cohesive-plus-contact model is quite similar with the basic idea in discrete element method (DEM) modelling in which two particles are linked with cohesion and friction, following Mohr-Coulomb rule.

The cohesive-plus-contact model is then further checked by the shear test with a constant normal compression but with various friction coefficients in the contacting surfaces, ranging from 0.3 to 0.9. The results demonstrate that while the cohesive stress remains almost unchanged, the total shear stress of the model is increased and the increase is in line with the increase of the friction effect.

3.2 Experimental verification

Having examined the working principles of the proposed cohesive-plus-contact model and the general effects of the key parameters, this section presents an experimental verification against a representative test on masonry specimens [25] to further validate the numerical model. As mentioned, the experiment was a triplet setup which is commonly used in the testing of masonry materials to determine the ultimate shear strength of the mortar joints. The failure mode is well controlled to the mortar joint interfacing two masonry blocks, and hence it provides a well-defined benchmark for the present verification purpose.

In the numerical model the brick parts are assumed to be elastic. The Young's modulus and density of the bricks are directly taken from the experiment, with E = 12 GPa and $\rho = 9.32 \times 10^{-4}$ g/mm^3. The Poisson's ratio is assumed to be 0.15 according to typical masonry material properties [20]. For the material properties of mortar joint between the bricks, the two key parameters, i.e. the critical (cohesive) stress and the friction coefficient, are directly obtained from the experimental data, and the values are $\sigma_I^P = \sigma_{II}^P = 0.25\ \text{MPa}$ and $\mu = 0.71$,which are fitted with Mohr-Coulomb relationship. The values for Mode-I and Mode-II fracture energy are taken from another shear test of masonry wall [26], i.e. $G_{IC} = 0.17\ \text{N/mm}$ and $G_{IIC} = 2.55\ \text{N/mm}$ as there is no direct data available.

The initial stiffness of the interface can be determined according to Eq. (1). Using the parameter $\alpha = 50$ and considering a mesh size 5 mm, $K_N = K_S = 1.2 \times 10^5$ MPa / mm. The static friction stress limit parameter is taken as two times of the cohesion strength in shear (i.e. $SFSL = 0.5$ MPa) according to the guideline discussed earlier, considering $\sigma_{II}^{P} = 0.25$ MPa and $\mu = 0.71$.

The comparison of the shear stress - shear displacement relationship between the experimental and the numerical simulation is illustrated in Figure 9. The numerical simulation results agree well with the experiments, and the predicted curves generally fit within the upper and lower bounds of the experimental data. The transition from cohesion to friction regime is very smooth, and the combined cohesive and friction model predicts correctly the pure friction stage.

The results from using only the cohesive element are also shown in Figure 9. As can be seen, the model fails to represent the dependency of the shear behaviour on the stress condition in the normal direction. This is attributable to an inability of such a model to deal with mixed-mode loading conditions, and the lack of a mechanism to maintain contact and prevent penetration after the failure of the cohesive elements. The proposed approach with a combination of cohesion and contact well resolves the penetration problem and allows the contact-friction to develop, and the final failure mode agrees very well with the experiment.

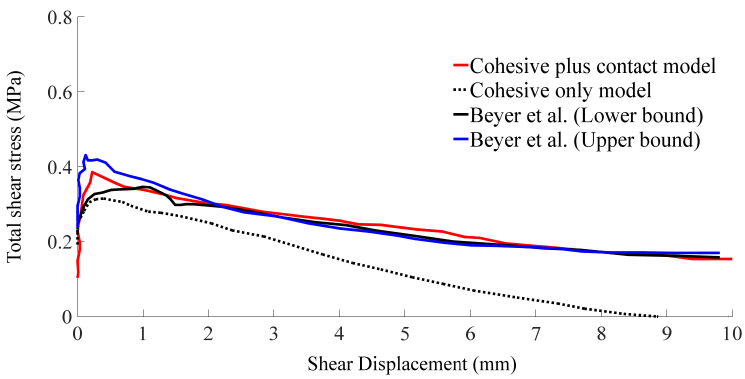

(a) Lateral pressure = 0.2 MPa

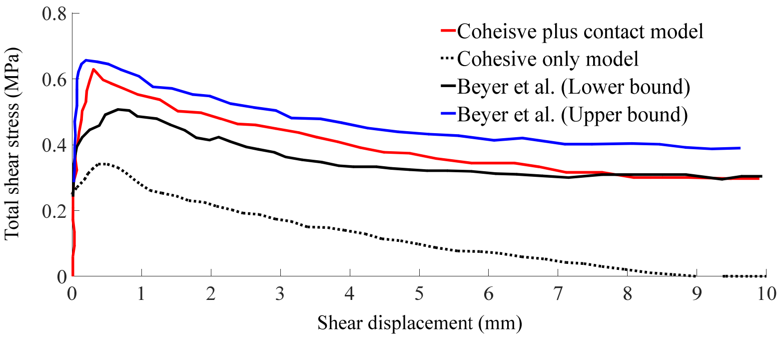

(b) Lateral pressure = 0.4 MPa

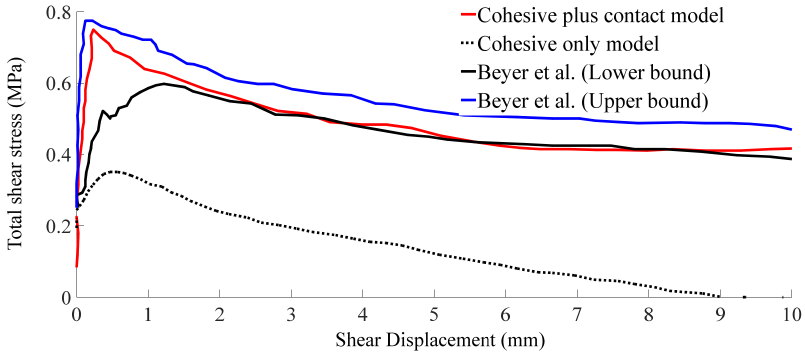

(c) Lateral pressure = 0.6 MPa

Fig. 9. Comparison of shear behavior with triplet tests by Beyer et al. [25] under different lateral pressures

4. Mesoscopic analysis of concrete incorporating the interface model

The proposed new interface approach is subsequently applied in the mesoscale concrete model framework. A standard cubic concrete specimen of 100 mm is modelled in a 2D plane stress setting. The model is subjected to both tension and compression loadings to examine its ability in simulating the damage evolution and the macroscopic response of concrete under different stress conditions.

In order to be able to produce the full range of the response of concrete including the softening stage, the analysis is carried using an explicit transient analysis scheme with LS-DYNA [27]. The loading is applied in a displacement-controlled manner through imposing a velocity boundary condition. The duration and pattern of the loading is carefully tuned such that the response resembles closely a quasi-static characteristic. More details of the loading scheme in the numerical simulation can be found in Tu and Lu [2].

4.1 Material parameters for mesoscale concrete

In the mesoscale model, the interface model with the combined cohesive and contact-friction components is used to model the fracture process at the interface between aggregates and mortar matrix, i.e., the ITZ.

The two bulk constituent materials, namely the aggregates and the mortar matrix, are modelled as continuum solids. Since the aggregate material is usually much stronger than mortar, it is reasonable to model the aggregates with a linear elastic material model. The mortar matrix may be represented by a damage-plasticity model to account for the damage and plastic deformation that may incur within the mortar matrix. Herein we use the K&C concrete damage model (material #72R3 in LS-DYNA) which has been calibrated extensively, including the controlling over the mesh dependency, in the literature [e.g. 2, 28]. It is also worth mentioning at this juncture that it is possible to extend the present cohesive-contact scheme to all element interfaces, including ITZ and mortar element, but obviously that would increase the computational cost.

All the material parameters here are assigned with values to represent a class of normal concrete with a compressive strength of 30 MPa. These material properties are determined based on data collected from relevant literature [29-30]. The material properties for aggregates include: E = 60 GPa, mass density $\rho = 2.6 \times 10^{-3}$g/mm^3, and the properties for mortar include: E = 30 GPa, $\rho = 2.3 \times 10^{-3}$g/mm^3 and compressive strength = 45 MPa. The Poisson's ratio is assumed to be 0.2 for both aggregate and mortar. The parameters used for the ITZ include normal peak traction $\sigma_I^P = 2.3$ MPa, energy release rate in mode-I $G_{IC} = 0.03\ \mathrm{N/mm}$ and the friction coefficient $\mu = 0.7$.

It should be noted here that the shear properties of ITZs, including the shear strength and the fracture energy in shear mode, are not precisely known in the literature. Therefore it is necessary to conduct parameter studies to find proper values for them, which will be given later.

Assuming the macroscopic elastic modulus of concrete with a nominal compressive strength 30 MPa is around 30 GPa [31], the initial stiffness of the interface can be estimated as $K_N = K_S = 1.5\times10^6$ MPa/mm according to Eq. (1), taking $\alpha = 50$. A refined mesh $h = 1$ mm, which is dictated by the need of discretising the mesoscale geometry of concrete, is adopted in the mesoscale model.

4.2 Parametrisation of other important material properties

For variable parameters which are difficult to determine from physical experiment, in particular the shear strength of the cohesive element S, the shear fracture energy G_{II} , and the friction stress limit parameter, a series of numerical simulations has been performed to examine their influences by comparing the macroscopic stress-strain relationship with relevant concrete experiments. Since these three parameters primarily influence model II cracking, and have little influence on the tension response, the parameterisation is conducted by examining the behaviour of the mesoscale model in quasi-static uniaxial compression.

The first parameter being examined here is the shear strength. The ratio between the shear and the normal critical traction (ST ratio) for a cohesive model is of particular importance for concrete. Experimental evidences [32-34] suggest that the peak strength is significantly larger in pure shear mode-II than in pure mode-I owing to the interlocking of aggregate particles in concrete. Swartz et al. [34] estimates the ST ratio (shear fracture strength to tensile strength) to range between 3 and 6 by analytical and numerical simulations of several mixed-mode tests.

Figure 10 shows the global stress-strain relationships in compression produced by the mesoscale model with different ST ratios. As can be seen, with an increase of the ST ratio, the compressive strength increases. For the targeted concrete of 30 MPa compressive strength, it appears that a ST ratio of 4 is appropriate for the cohesive material. This value is slightly lower than the one chosen in [11] in which a ST value of 5 was used for a homogeneous concrete model. It is worth noting that aggregate interlocking in the later contact-friction stage is largely represented in the current mesoscale by the explicit inclusion of the aggregates in the model.

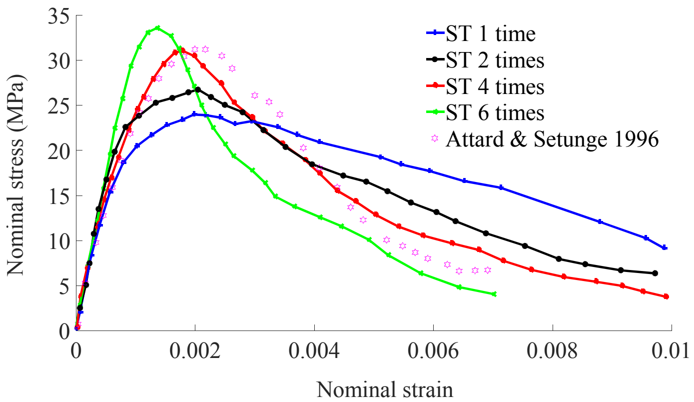

Fig. 10. Influence of shear strength of cohesive element for concrete under compression (*SE* = 10 and *SFLS* = $2\sigma_{II}^{P}$)

It is also interesting to observe that the cohesive shear strength also has an influence on the damage patterns, which relate to the softening behaviour. As shown in Figure 11, the final cracking patterns are markedly different for the lower shear strength cases (ST ratio of 1 or 2) as compared to the higher shear strength case (ST ratio of 3). The final damage pattern from the higher shear strength case agrees very well with experimental evidence [35] and the numerical result by other researchers [29].

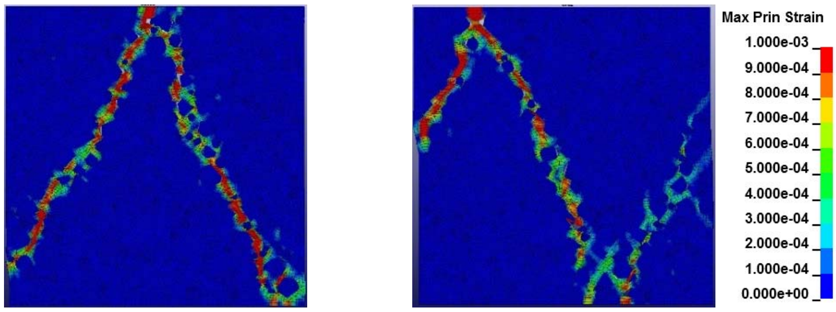

(a) ST = 2 (b) ST = 4

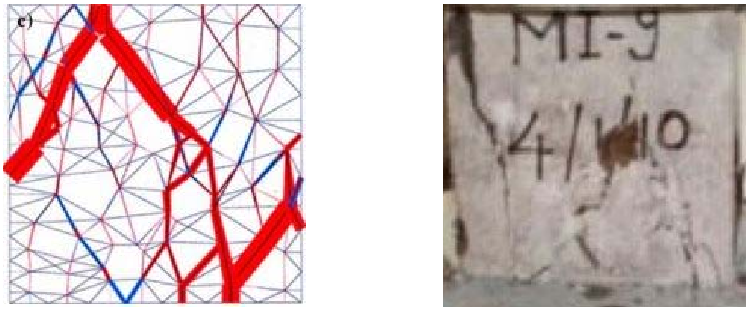

(c) Lopez et al. [29] (d) Fatima et al. [35]

Fig. 11. Crack patterns (principle strain) under compression with different cohesive shear strengths

The next factor examined is the fracture energy ratio between the Mode-II and the Mode-I for the cohesive model, herein referred to as SE ratio. Experimental observations generally suggest that the fracture energy in pure mode-II is much larger than in tension mode-I [36]. However there is a large scatter in the specific SE ratios used by different researchers, for examples, 8 to 10 by Swartz, et al. [37] but around 25 by Bažant and Pfeiffer [38].

Figure 12 shows the global stress-strain relationships for the model with different SE ratios. As can be seen, with a higher value of G_{II}, the dissipated fracture energy increases and thus modifies mostly the post-peak behaviour and shifts the transition to softening towards higher strain value. A SE value of 10 appears to be appropriate in the current mesoscale framework as it leads to the strain at peak strength of around 0.002 which is typical for normal concrete under uniaxial compression. This choice is on the lower end of the experimental evidence as mentioned earlier, and is deemed reasonable considering the fact that the geometric aspect of the aggregate interlocking is already represented in the present mesoscale model.

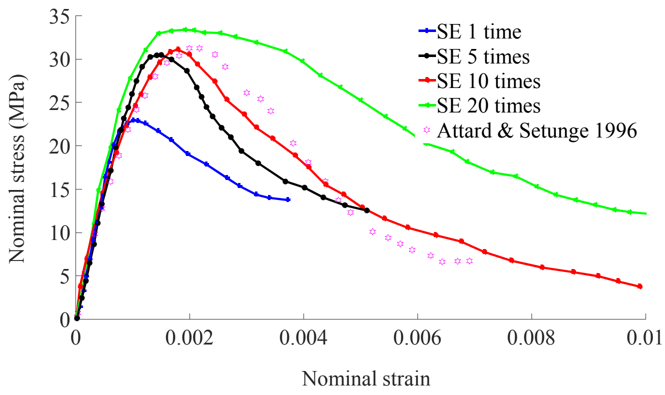

Fig. 12. Influence of shear fracture energy (*ST* = 4 and *SFSL* = $2\sigma_{II}^{P}$)

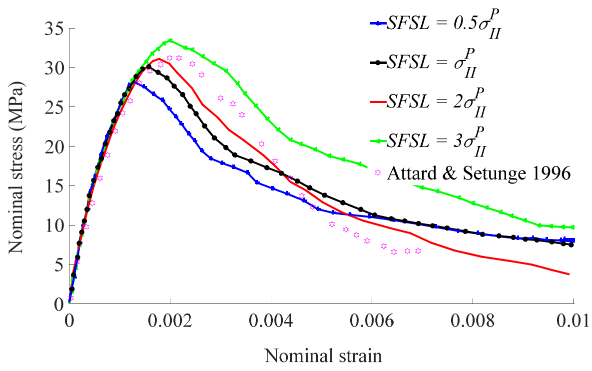

Fig. 13. Influence of friction limit *SFLS* (*ST* =4 and *SE* = 10)

As discussed earlier, the static friction limit *SFSL* is a key parameter in the cohesive-plus-contact model and it controls the static friction mechanism before de-cohesion. Preliminary numerical analysis tends to suggest a limit value of *SFSL* equal to two times of the cohesion strength. The adequacy of this in the mesoscale model is further examined herein. Figure 13 shows the nominal compressive stress-strain curves for different values of *SFSL*. The results confirm that the value of two times of cohesion is appropriate for the mesoscale concrete model as well.

4.3 Simulation of uniaxial tension

The cubic mesoscale numerical specimen is subjected to axial tension. Figure 14 illustrates the development of the cracks. The damage is illustrated by the axial tensile strain in the range of (0, 0.001), with the upper bound signifying open cracks. It can be observed that upon the peak stress many micro-cracks have developed and are located mostly at the interface between aggregates and mortar. As the deformation increases, concentrated macro cracks starts to emerge, and this brings the specimen into the softening stage. Because of the stress relief, unloading and recovery of the elastic deformation takes place in the areas outside the macro crack. Many small micro-cracks stop opening further. With further increase of the applied tensile deformation, the concentrated macro cracks propagate transversely, cutting through the ITZ region, and finally coalesce to form virtually a single crack across the entire width of the specimen. This phenomenon is a reproduction of what has been observed generally in direct tension experiments.

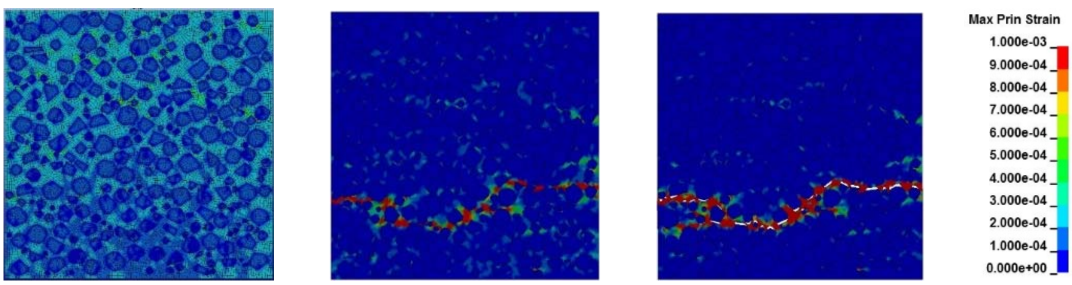

(a) Before peak load (b) Around peak (c) Final crack pattern

Fig. 14. Crack patterns in tension: (a) Before peak load; (b) Around peak; (c) Final pattern

The corresponding tensile stress-strain curve is given in Figure 15 in comparison with the experimental data [39]. For comparison the tensile stress-strain curve produced with a model without involving the contact mechanism is also presented. It can be seen that the stress-strain curve from the cohesive-plus-contact model gives almost the same result as the pure cohesive model under an axial tension. This is because almost no contact-frictional mechanism is involved in a direct tension situation. The tensile strength is around 3 MPa, as expected, with a corresponding peak strain 120 microstrain which is consistent with experimental observations.

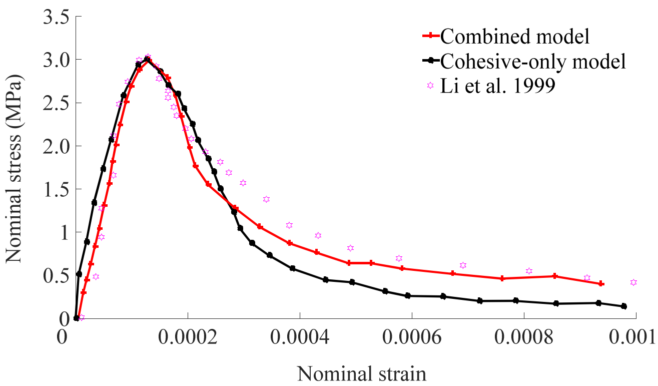

Fig. 15. Stress strain curves in tension

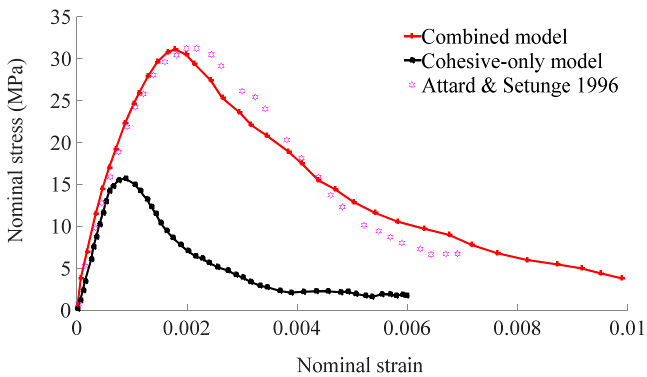

Fig. 16. Stress-strain curves in uniaxial compression

4.4 Simulation of uniaxial compression

A perfect uniaxial compression, without any lateral constraint on the loading faces, is simulated herein. The results are compared in Figure 16. The inherent problem with the cohesion-only model becomes apparent; such a model fails to achieve satisfied either the compressive strength or the softening response. The cohesive-plus-contact model, on the other hand, predicts well the experimental curve both in terms of the strength and deformation, including the softening stage of the response.

4.5 Compression with lateral confinement

The compressive behaviour of concrete is known to be sensitive to the lateral confinement. Generally with the increase of the lateral confinement pressure, both the compressive strength and the ductility show significant enhancement.

Simulations of the compressive behaviour of the concrete specimen under different levels of confining pressure, at 1.5, 4.5, and 9.0 MPa, respectively, have been performed. The confining pressure is applied as inward lateral force on the two sides of the specimen. Figure 17 illustrates the nominal axial stress-strain responses of the specimens under the different confining pressures. The experimental data from triaxial loading tests reported in Sfer et al. [40] are selected for a direct comparison.

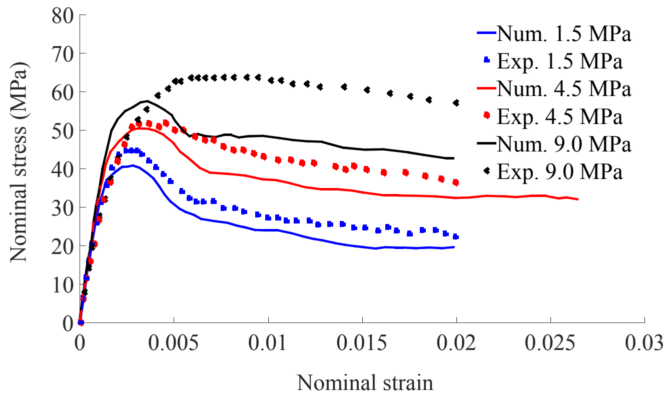

Fig. 17. Confinement effects

The simulation results agree favourably with the experimental data. As expected the compressive strength of the concrete increases markedly with an increase of the confining pressure. The lateral confinement also results in an increase in the ductility of the concrete material, which also shows a reasonable agreement between the numerical and experimental results. It can be seen that difference between the model and experimental data appear to increase with the lateral confinement. This is believed to relate to the limitation of a 2D model in representing the full lateral confinement effect, and may only be properly resolved when the proposed cohesive plus contact approach is implemented in 3D mesoscale concrete model, which should be a subject for the future study.

5. Dynamic compression

Classical experimental results have shown that the "apparent" dynamic compressive strength of concrete increases with the increase of the strain rate, and such an increase is generally defined by a Dynamic Increase Factor. However, the true mechanism underlying the occurrence of the DIF is still a subject of continued debate. Various analytical and numerical studies in more recent years, including an analysis using a 3D mesoscale model [41], provided detailed results showing the predominant contribution of the lateral inertial confinement in the increase of the dynamic compressive strength.

In this section the new 2D mesoscale model with cohesive-plus-contact interface for the ITZ is employed to simulate the dynamic compression. With an explicit representation of the ITZ, the mesoscale model is expected to describe the dynamic fracture process and its influences more directly, and thus provides additional insight into the dynamic behaviour of the concrete material.

For a comparison, a 2D homogeneous model and a 2D mesoscale model with an equivalent solid ITZ layer are also analysed for the same variation range of the strain rates. To facilitate a direct observation of the contribution of the structural inertial effects, all the constituent materials are considered to be rate insensitive, i.e, no embedded strain rate enhancement factor is adopted in the material properties in all the models. This means any increase in the apparent compressive strength of the simulated test specimen is attributable to the structural effect, including the inertial confinement and the dynamic interface contact mechanisms, as well as the material heterogeneities.

A similar displacement controlled loading via a velocity boundary condition as in the quasi-static analysis is used in the dynamic simulation, but a higher velocity and a shorter time duration is adopted in order to achieve a desirable strain rate.

For the current concrete specimen of 100 mm size, a strain rate range of up to 100 /s is simulated. Further increased strain rate would cause excessive stress wave effect which may only be minimized with the use of smaller specimens [42]. The average stress on the loading and supporting faces is extracted from the numerical results, from which the peak values are identified which represent the dynamic strength of the specimen. The ratio between the dynamic strength and the quasi-static strength (30 MPa herein) is then obtained as the DIF for each strain rate.

Figure 18(a) plots the DIF vs. strain rate curves based on the simulation results from the three models. It can be observed that all models exhibit an increase in the nominal compressive strength as the strain rate increases, despite that no strain rate enhancement has been incorporated in the material constitutive model. The general trend of the simulated DIF curves resembles well the curves given by the empirical formula in CEB-FIP [43]. The cohesive-plus-contact model exhibits an improved agreement with the empirical curve, and this is deemed to be attributable to a comprehensive representation of the various mechanisms that could affect the failure process under a dynamic compression, including the contact-friction mechanism in addition to the effects of the inertial confinement and the presence of the aggregates.

Representative damage and crack patterns under different strain rates are provided in Figure 18(b). One can notice that with the increase of the loading rate, the number of micro-cracks also increases. Cracks tend to propagate within the matrix phase bypassing the aggregate inclusions within the strain rate range under consideration.

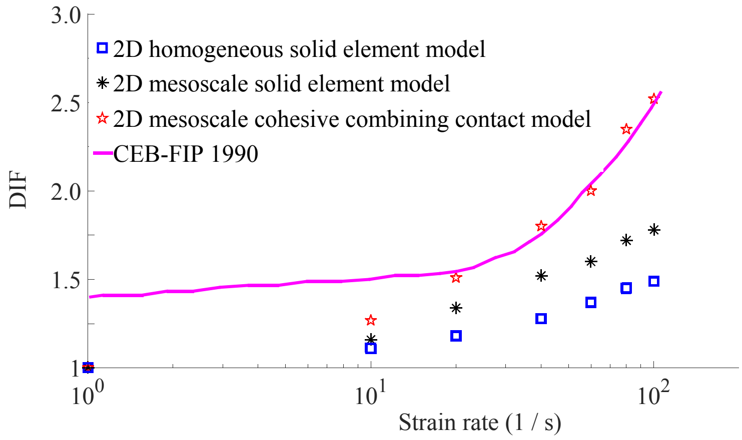

(a) DIF curves

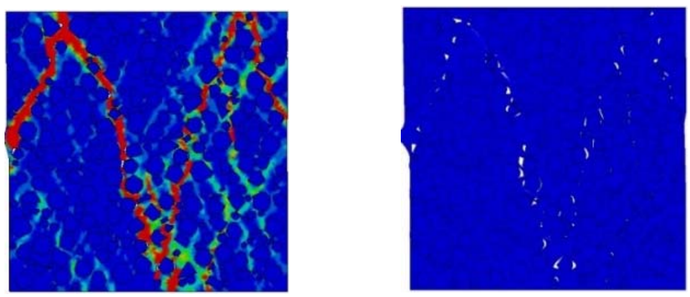

(b) Damage pattern under strain rate 10 /s

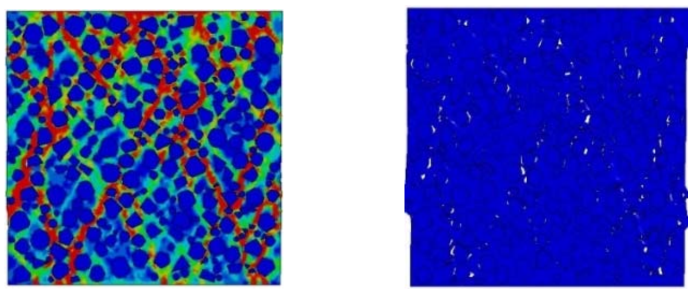

(c) Damage pattern under strain rate 100 /s

Fig. 18. DIF vs. strain rate results and associated damage patterns for combined cohesive-contact model

6. Conclusions

In this paper, a 2D mesoscale concrete model incorporating a combined cohesive and contact-friction interface for the ITZ has been presented. The contact-friction mechanism is modelled as an independent mechanism which works alongside the classical cohesive approach. The general behaviour of the combined cohesive and contact-friction interface approach is first verified in a triplet shear configuration with varying lateral pressure. The results show that the model is capable of representing the physical process of shear resistance in the presence of lateral pressure, and a smooth transition from nucleation of cracks to the pure frictional state can also be realised.

The cohesive-plus-contact interface model is then implemented in the 2D mesoscale concrete model. Adding onto a realistic description of the topology of the fracture path from the mesoscale model, the interface approach enables a more realistic simulation of the complex fracture and degradation process in concrete suitable for different loading conditions. A parameter investigation is conducted to examine the influence of the shear properties for the ITZ, for which the experimental data are generally lacking, on the macroscopic responses of concrete. The model is then validated against relevant experimental results under uniaxial tension, uniaxial compression, and compression with lateral confinement.

As an application, the model is subsequently applied in the simulation of dynamic compression under high strain rates. The simulation results show a good agreement with empirical data in terms of the increase of the dynamic strength with the strain rate and the damage patterns.

The mesoscale model with the proposed cohesive-plus-contact model provides a comprehensive numerical tool for investigation into the micro-mesoscale mechanisms underlying the bulk properties of concrete material. It can be employed to assist in the material investigation as well as characterisation of the material behaviour in complex loading conditions.

It should be noted that in the current mesoscale model, the cohesive-plus-contact elements have been employed only for the ITZ layer surrounding the aggregates. As such the model can explicitly simulate fracture and fracture-induced discontinuity across the ITZ, which is known to play a key role in the damage process of concrete. However, the fracture and damage within concrete can extend into the mortar matrix, and can even occur within aggregates under extreme loading such as high rate tension. To facilitate a full simulation of fracture process in concrete, a model allowing for discontinuity and friction mechanisms to develop in all three mesoscale parts, i.e. aggregates, mortar and ITZ, will be needed. This is a topic that warrants further research and the progress in that direction will be reported separately.

ACKNOWLEDGEMENTS

The research reported in the paper is partly funded by the Chinese Scholarship Council and the University of Edinburgh through a joint scholarship for the PhD study of the first author.

REFERENCES

[1] Wriggers, P., and Moftah, S. Mesoscale models for concrete: Homogenisation and damage behaviour. *Finite elements in analysis and design* 2006; 42(7): 623-636.

[2] Tu, Z., and Lu, Y. Mesoscale modelling of concrete for static and dynamic response analysis-Part 1: model development and implementation. *Structural Engineering and Mechanics* 2011; 37(2): 197-213.

[3] Wang, X., Yang, Z. J, Yates, R., Jivkov, A.P., Zhang C. Monte Carlo simulations of mesoscale fracture modelling of concrete with random aggregates and pores. Constr Build Mater 2015; 75: 35-45.

[4] Lu Y. Modelling the dynamic response of concrete with mesoscopic heterogeneity. In *Understanding the Tensile Properties of Concrete* (Ed. J. Weerheijm), Chapter 8,

Woodhead Publishing Limited. 2013:218-267.

[5] Hwang, Y. K., Bolander, J. E., Lim, Y. M. Simulation of concrete tensile failure under high loading rates using three-dimensional irregular lattice models. *Mechanics of Materials* 2016; 101: 136-146.

[6] Lilliu, G., and van Mier, J. G. 3D lattice type fracture model for concrete. *Engineering Fracture Mechanics* 2003; 70(7): 927-941.

[7] López, C. M., Carol, I., Aguado, A. Meso-structural study of concrete fracture using interface elements. I: numerical model and tensile behavior. *Materials and structures* 2008; 41(3): 583-599.

[8] Kregting, R. Cohesive zone models: towards a robust implementation of irreversible behavior. Dissertation, Eindhoven University of Technology, The Netherlands, 2005.

[9] Nitka, M., and Tejchman, J. Modelling of concrete behaviour in uniaxial compression and tension with DEM. *Granular Matter* 2015; 17(1): 145-164.

[10] Scrivener, K. L., Crumbie, A. K., Laugesen, P. The interfacial transition zone (ITZ) between cement paste and aggregate in concrete. *Interface Science* 2004; 12(4): 411-421.

[11] Ruiz, G., Pandolfi, A., Ortiz, M. Three‐dimensional cohesive modeling of dynamic mixed‐mode fracture. *International Journal for Numerical Methods in Engineering* 2001; 52(1-2): 97-120.

[12] Wang, Z., Kwan, A., Chan, H. Mesoscopic study of concrete I: generation of random aggregate structure and finite element mesh. *Computers & Structures* 1999; 70(5): 533-544.

[13] Snozzi, L., Caballero, A., Molinari, J.-F. Influence of the meso-structure in dynamic fracture simulation of concrete under tensile loading. *Cement and Concrete Research* 2011; 41(11): 1130-1142.

[14] Gerlach, S., Fiolka, M., Matzenmiller, A. Modelling and analysis of adhesively bonded joints with interface elements for crash analysis." *Proceedings of the LS-DYNA conference,* Bamberg, 2005.

[15] Vulovic, S., Zivkovic, M., Grujovic, N. Contact Problems Based on the Penalty Method. *Scientific Technical Review* 2008; 63(3-4): 2126-2132.

[16] Tvergaard, V. Effect of fibre debonding in a whisker-reinforced metal. *Materials Science and Engineering: A* 1990; 125(2); 203-213.

[17] Chaboche, J., Girard, R., Schaff, A. Numerical analysis of composite systems by using interphase/interface models. *Computational Mechanics* 1997; 20(1-2): 3-11.

[18] Koutromanos, I., and Shing, P. Cohesive crack model to simulate cyclic response of concrete and masonry structures. *ACI Structural Journal* 2012; 109(3): 349-358.

[19] Sacco, E., and Toti, J. Interface elements for the analysis of masonry structures. *International Journal for Computational Methods in Engineering Science and Mechanics* 2010; 11(6): 354-373.

[20] Alfano, G., and Sacco, E. Combining interface damage and friction in a cohesive‐zone model. *International Journal for Numerical Methods in Engineering* 2006; 68(5): 542-582.

[21] Turon, A., Davila, C. G., Camanho, P. P., Costa, J. An engineering solution for mesh size effects in the simulation of delamination using cohesive zone models. *Engineering fracture mechanics* 2007; 74(10): 1665-1682.

[22] Turon, A., Camanho, P. P., Costa, J., Dávila, C. A damage model for the simulation of delamination in advanced composites under variable-mode loading. *Mechanics of Materials* 2006; 38(11): 1072-1089.

[23] Nakamura, H., Tran, K., Kawamura, K., Kunieda, M. Crack propagation analysis due to

rebar corrosion. *Proc. The 7th International Conference on Fracture Mechanics of Concrete and Concrete Structures (FramCoS-7),* Korea, 2010: 921-928.

[24] Vandewalle, L. RILEM TC 162-TDF: Test and design methods for steel fibre reinforced concrete. *Materials and Structures* 2000; 33(225): 3-6.

[25] Beyer, K., Abo-El-Ezz, A., Dazio, A. *Quasi-static cyclic tests on different types of masonry spandrels*, vdf Hochschulverlag AG an der ETH Zürich, 2010.

[26] Pina-Henriques, J., and Lourenço, P. B. Masonry compression: a numerical investigation at the meso-level. *Engineering computations* 2006; 23(4): 382-407.

[27] LS-DYNA keyword user's manual version 971. *Livermore Software Technology Corporation*, 2007.

[28] Tu, Z., and Lu, Y. Evaluation of typical concrete material models used in hydrocodes for high dynamic response simulations. *International Journal of Impact Engineering* 2009; 36(1): 132-146.

[29] López, C. M., Carol, I., Aguado, A. Meso-structural study of concrete fracture using interface elements. II: compression, biaxial and Brazilian test. *Materials and Structures* 2008; 41(3): 601-620.

[30] Nagai, K., Sato, Y., Ueda, T. Mesoscopic simulation of failure of mortar and concrete by 2D RBSM. *Journal of Advanced Concrete Technology* 2004; 2(3): 359-374.

[31] ACI. Building code requirements for structural concrete (ACI 318-08) and commentary. American Concrete Institute, 2008.

[32] Cedolin, L., Bisi, G., Nardello, P. Mode II fracture resistance of concrete. *Concrete Science and Engineering* 1999; 1(1): 37-44.

[33] Jia, Z., Castro-Montero, A., Shah, S. Observation of mixed mode fracture with center notched disk specimens. *Cement and Concrete research* 1996; 26(1): 125-137.

[34] Swartz, S., and Taha, N. Crack propagation and fracture of plain concrete beams subjected to shear and compression. *Structural Journal* 1991; 88(2): 169-177.

[35] Fatima, E., Jhamb, A., Kumar, R. Ceramic dust as construction material in rigid pavement. *American Journal of Civil Engineering and Architecture* 2013; 1(5): 112-116.

[36] Achintha, M., and Burgoyne, C. Fracture energy of the concrete–FRP interface in strengthened beams. *Engineering Fracture Mechanics* 2013; 110: 38-51.

[37] Swartz, S., Lu, L., Tang, L., Refai, T. Mode II fracture-parameter estimates for concrete from beam specimens. *Experimental Mechanics* 1988; 28(2): 146-153.

[38] Bažant, Z., and Pfeiffer, P. Shear fracture tests of concrete. *Materials and Structures* 1986; 19(2): 111-121.

[39] Li, Q., and Ansari, F. Mechanics of damage and constitutive relationships for high-strength concrete in triaxial compression. *Journal of engineering mechanics* 1999; 125(1): 1-10.

[40] Sfer, D., Carol, I., Gettu, R., Etse, G. Study of the behavior of concrete under triaxial compression. *Journal of Engineering Mechanics* 2002; 128(2): 156-163.

[41] Lu, Y., and Zhou, R. A 3-D perspective of dynamic behaviour of heterogeneous solids. *Proc., EPJ Web of Conferences*, EDP Sciences, 04038, 2015.

[42] Song, Z. H., and Lu. Y., Mesoscopic analysis of concrete under excessive high strain-rate compression and implications on interpretation of test data. *Int J Impact Eng*. 2012; 46: 41-55.

[43] CEB-FIP Model Code 1990, Evaluation of the time dependent behavior of concrete. Redwood Books, Trowbridge, Wiltshire, UK, 1993.